Emission Mechanism of Polyatomic Ions Cs2Cl+ and Cs2BO2+ in Thermal Ionization Mass Spectrometry with Various Carbon Materials

8 AUTHORS, INCLUDING:

Shao-Yong Jiang
Nanjing University
232 PUBLICATIONS **3,227** CITATIONS

Tao Yang
Nanjing University
23 PUBLICATIONS **204** CITATIONS

Xiong Yan
Nanjing University
6 PUBLICATIONS **18** CITATIONS

Emission Mechanism of Polyatomic Ions Cs_2Cl^+ and $Cs_2BO_2^+$ in Thermal Ionization Mass Spectrometry with Various Carbon Materials

Hai-Zhen Wei,[†] Shao-Yong Jiang,*,[†] Gary N. Hemming,[‡,§] Jing-Hong Yang,[†] Ying-Kai Xiao,[†,⊥] Tao Yang,[†] Xiong Yan,[†] and Yan Yan[†]

[†]State Key Laboratory for Mineral Deposits Research, Department of Earth Sciences, Nanjing University, Nanjing 210093, People's Republic of China

[‡]Department of Earth and Environmental Sciences, Lamont-Doherty Earth Observatory of Columbia University, Palisades, New York 10964−8000, United States

[§]Queens College School of Earth and Environmental Sciences, Flushing, New York 11367, United States

[⊥]Qinghai Institute of Salt Lakes, Chinese Academy of Sciences, Xining 810003, People's Republic of China

ABSTRACT:
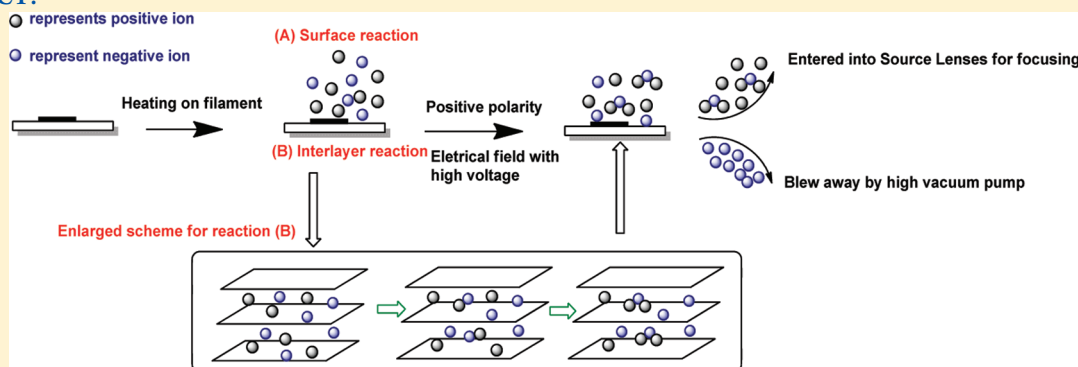
The emission behavior of polyatomic ions Cs_2Cl^+ and $Cs_2BO_2^+$ in the presence of various carbon materials (Graphite, Carbon, SWNTs, and Fullerenes) in the ionization source of thermal ionization mass spectrometry (TIMS) has been investigated. The emission capacity of various carbon materials are remarkably different as evidenced by the obvious discrepancy in signal intensity of polyatomic ions and accuracy/precision of boron and chlorine isotopic composition determined using Cs_2Cl^+-graphite-PTIMS/$Cs_2BO_2^+$-graphite-PTIMS methods. Combined with morphology and microstructure properties of four selected carbon materials, it could be concluded that the emission behavior of the polyatomic ions strongly depends on the microstructure of the carbon materials used. A surface-induced collision mechanism for formation of such kinds of polyatomic ions in the ionization source of TIMS has been proposed based on the optimized configuration of $Cs_2BO_2^+$ and Cs_2Cl^+ ions in the gas phase using a molecular dynamics method. The combination of the geometry of the selected carbon materials with the configuration of two polyatomic ions explains the structure effect of carbon materials on the emission behavior of polyatomic ions, where graphite samples with perfect parallels and equidistant layers ensure the capacity of emission to the maximum extent, and fullerenes worsen the emission of polyatomic ions by blocking their pathway.

INTRODUCTION

Small polyatomic ions, such as H_xCO^+ and $H_xN_2^+$, have been observed in inductively coupled plasma mass spectrometry,[1] and polyatomic hydrocarbon ions were produced from the chemical reaction of radical cation projectiles with highly oriented pyrolytic graphite surface.[2] The mechanism of collision-induced dissociation/surface-induced dissociation of polyatomic projectile ions has been proposed by Laramhe et al. by using the technique of angle-resolved mass spectrometry.[3,4] Larger polyatomic ions, such as $Na_2BO_2^+$ and $Cs_2BO_2^+$, were observed in the ionization source of thermal ionization mass spectrometry (TIMS) and then were employed for the isotopic composition measurement of boron since 1948.[5−7] The $Cs_2BO_2^+$-PTIMS (positive thermal ionization mass spectrometry) method had been greatly
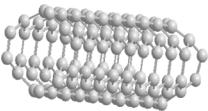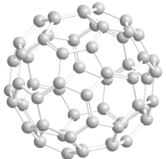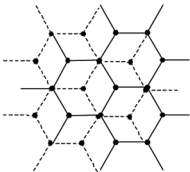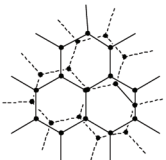
improved by Xiao et al. who found the intensity of $Cs_2BO_2^+$ emitted from $Cs_2B_4O_7$ can be increased to two-orders of magnitude when loading graphite on the filament in TIMS at low temperature (<400 °C)[8] and it was estimated as one of the best methods for the determination of boron isotopic composition with the highest precision of 0.1‰ (1σ) for natural samples.[9] Later on, a highly precise isotopic measurement procedure by TIMS for chlorine,[10] bromine[11] had been established, and that of nitrogen and oxygen in nitrate salt was explored as well[12] by detecting the polyatomic ions Cs_2Cl^+, Cs_2Br^+, and $Cs_2NO_2^+$ that are only

Table 1. Overall Views of SWNTs and C_{60} Structures and Top Views of Graphite and Carbon As Well As Their Hybridized Orbital of Carbon Bonds

Carbon Type	Microstructure	Hybridized Orbital	Structure Parameters
SWNT		sp^2	Bond length: C-C: 0.145 nm; C=C: 0.140 nm Tube diameter: ~ 1-2 nm
C_{60}		sp^2	Average C-C bond length: 0.142 nm Ball diameter: 0.71 nm
Graphite		sp^2	Intraplanar C-C bond length: 0.142 nm Interplanar space distance: 0.3354 nm
Carbon		~85 % sp^2	Intraplanar C-C bond length: 0.142 nm Interplanar space distance: 0.344 nm

formed in the presence of graphite. Compared with small poly-atomic ions from covalent compounds, the formation mechanism of $M_2X^+/M_2BO_2^+/M_2CNO^+$ type polyatomic ions (M denotes alkali metal, e.g., Na, K, Rb, Cs, and X is a halogen, e.g., Cl, Br, I) obtained from electrovalent compounds in the ionization source of TIMS has not been investigated so far, and the understanding of the surface reaction mechanism of the associative ion will be a great challenge.

Carbon occurs in many forms and due to the dependence of the properties of each form on its special structure, carbon has been investigated for more than half a century without exhausting its wonders and challenges as reviewed by Dresselhaus.[13] Common carbon materials with large specific surface area (sometimes called active, amorphous, or microcrystalline carbon) are assuming increasing importance in various fields, such as in control of pollution, in purifying and controlling general chemical environment, and in certain biomedical applications.[14] All applications of carbon involve adsorption and catalysis, physical-chemical processes which may depend upon the crystalline structure, microscopic physical structure, electronic properties, surface chemistry, as well as the presence of impurities within the carbon. Except for the classical graphitizable carbon (i.e., graphite) and turbostratic carbon (i.e., amorphous carbon) we mentioned above, other sp^2-hybridized carbon materials with unique structures, such as novel nanotubes (e.g., single-walled nanotubes, SWNTs, and multiply walled nanotubes, MWNTs) with excellent performance in mechanical stiffness, electrical and thermal conductivity, and optical properties[15] and polymerized fullerenes (e.g., C_{60} or C_{70}) with unique electrical and photophysical properties[16] have been widely investigated/employed in nanotechnology and nanoscience, such as electron-accepting component, photoelectrochemical/photosynthetic models, hydrogen

storage component, drug-delivery, and therapeutic agents etc.[17−25]

In our previous investigation, the emission behavior of larger polyatomic ions with various graphite and carbon samples has been compared, which suggested that the presence of a graphite promoter plays a key role for the formation of polyatomic ions and the characterization on the differences in planar crystalline structure confirmed the relationship between the emission capacity of polyatomic ions and the crystal microstructure of graphite.[26] Considering the dramatic differences in microstructure among graphite, carbon, SWNTs, and C_{60} even though the same sp^2 hybridized orbital existed in the majority in all of them (Table 1), the question of how other carbon materials with unique microstructure influence on the emission of such polyatomic ions raises our attention to explore the real formation mechanism in TIMS.

To present the direct evidence for the above statement, experimental characteristics on the morphology and microstructure of four kinds of typical carbon materials (i.e., graphite, carbon, SWNTs, and C_{60}) are preformed by using transmission electron microscopy (TEM) and Raman spectroscopy in this study. The relationship between the emission capacity of polyatomic ions and the microstructure of various carbon materials, and the surface-induced collision mechanism for the formation of polyatomic ions, as well as the structure effect of carbon materials on the emission behavior of polyatomic ions will be discussed in detail in this work.

2. EXPERIMENTAL SECTION

2.1. Chemicals and Reagents. High-purity graphite, nano-carbon with average particle size of 700 nm in diameter, single-walled nanotubes (SWNT) with 99% purity, C_{60} with 85% purity

Table 2. Source and the Purity of Four Selected Carbon Materials

no.	type	origin	purity
1	graphite	Johnson−Matthew Company, USA	highly pure, 99.9999%
2	carbon	Shanghai Carbon Factory, P. R. China	spectral purity, ash:0.005%
3	single-walled nanotubes (SWNTs)	Fujian Institute of Research on the Structure of Matter, Chinese Academy of Sciences, P. R. China	99% purity
4	fullerenes (C$_{60}$)	Fujian Institute of Research on the Structure of Matter, Chinese Academy of Sciences, P. R. China	∼85% purity

(a) Fullerenes (C$_{60}$)   (b) Single walled nanotubes (SWNT)
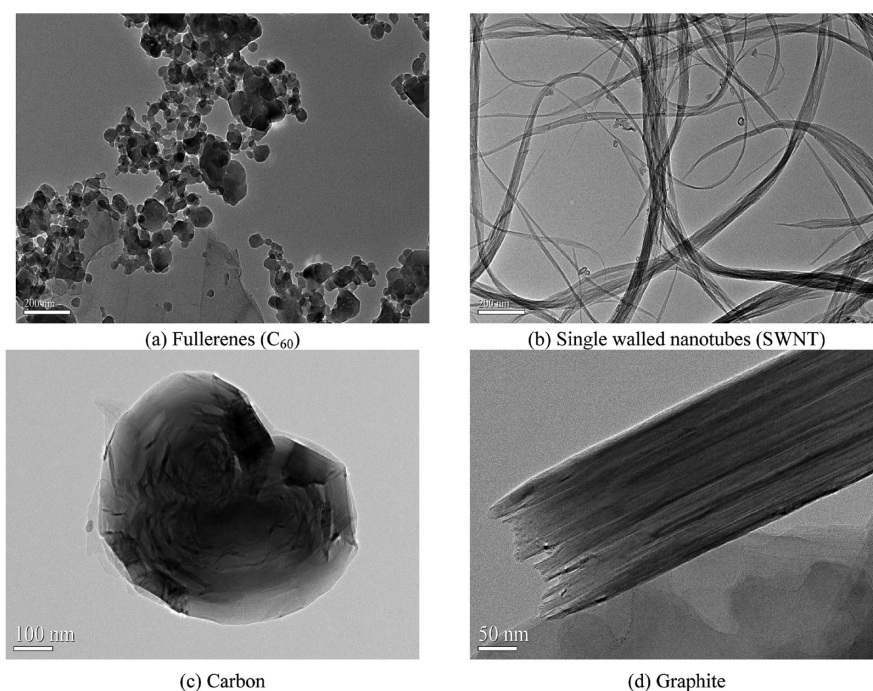
(c) Carbon   (d) Graphite

Figure 1. TEM images of various carbon materials: (a) fullerenes (C$_{60}$); (b) single-walled nanotubes (SWNT); (c) nanocarbon; and (d) graphite.

obtained from different sources were selected in the experiment (Table 2). All fine carbon powder materials were used as received without further purification. They were mixed in 80% ethanol/20% water (v/v) to form slurry for boron and chlorine isotopic measurement by TIMS. Ultra pure deionized-filtered water (Millipore, resistivity, 18.2 MΩ cm) was used in the whole experiment. Solution of Cs-borate (1 μg/μL B and molar ratio of B/Cs 2:1) was prepared by NIST SRM 951 boric acid and Cs$_2$CO$_3$ reagents, and neutral solution of CsCl containing 1 μg/μL Cl was converted from NIST SRM 975 NaCl using Cs$^+$-cation resin for the measurement of boron and chlorine isotopic compositions, respectively.

2.2. Methods and Instruments. A Triton thermal ionization mass spectroscopy (Triton Ti) has been used for the analysis of isotopic compositions of boron and chlorine. Single tantalum and rhenium filaments (0.75 × 0.076 ×0.0025 cm) from NIST were degassed in vacuum for 1 h at current 3.0 A. The filaments were then allowed to oxidize in the ambient atmosphere (protected from contamination in closed boxes) for at least 24 h prior to use, which improves the working function of metal filament to expedite the emission of positively charged ions.[27,28] The carbon material slurry of 1.0 μL was first loaded onto the filament, and then the sample solution followed after vaporizing the slurry drop

at room temperature for 30 s. The analytical methods for the chlorine and boron isotopic determination has followed the procedures reported by Xiao et al.[8,10] The static measurement of boron isotopic composition by PTIMS-graphite-Cs$_2$BO$_2$$^+$ method has been established by collecting ^{133}Cs$_2$^{10}B^{16}O$_2$$^+$ (m/e 308) at H3 cup and ^{133}Cs$_2$^{11}B^{16}O$_2$$^+$ (m/e 309) at H4 cup and the adjustment of the parameters in Zoom Optics at the commercial software of Triton Ti ensures the perfect overlap of the peak at m/e 308 and that at m/e 309.[29]

Raman spectra of graphite samples were recorded using JY-HR 800 Raman spectrometer equipped with 488 nm wavelength green laser (<1mW) in the range of 50−3000 cm^{-1}. Transmission electron microscopy (TEM) was performed on a JEOL JEM-2100 microscope operated at an acceleration voltage of 200 kV. Each fine powder of carbon samples was well dispersed in ethanol with supersonic method and a drop of carbon-ethanol slurry solution was added on a carbon coated microscope grid (400 meshes from SPI) with a micropipe. After holding the sample solution on the grid for 20 s, the drop remaining was quickly removed by momentary contact of a filter paper, which keeps the dried sample layer in a proper thickness for transmission of electron beam in TEM.
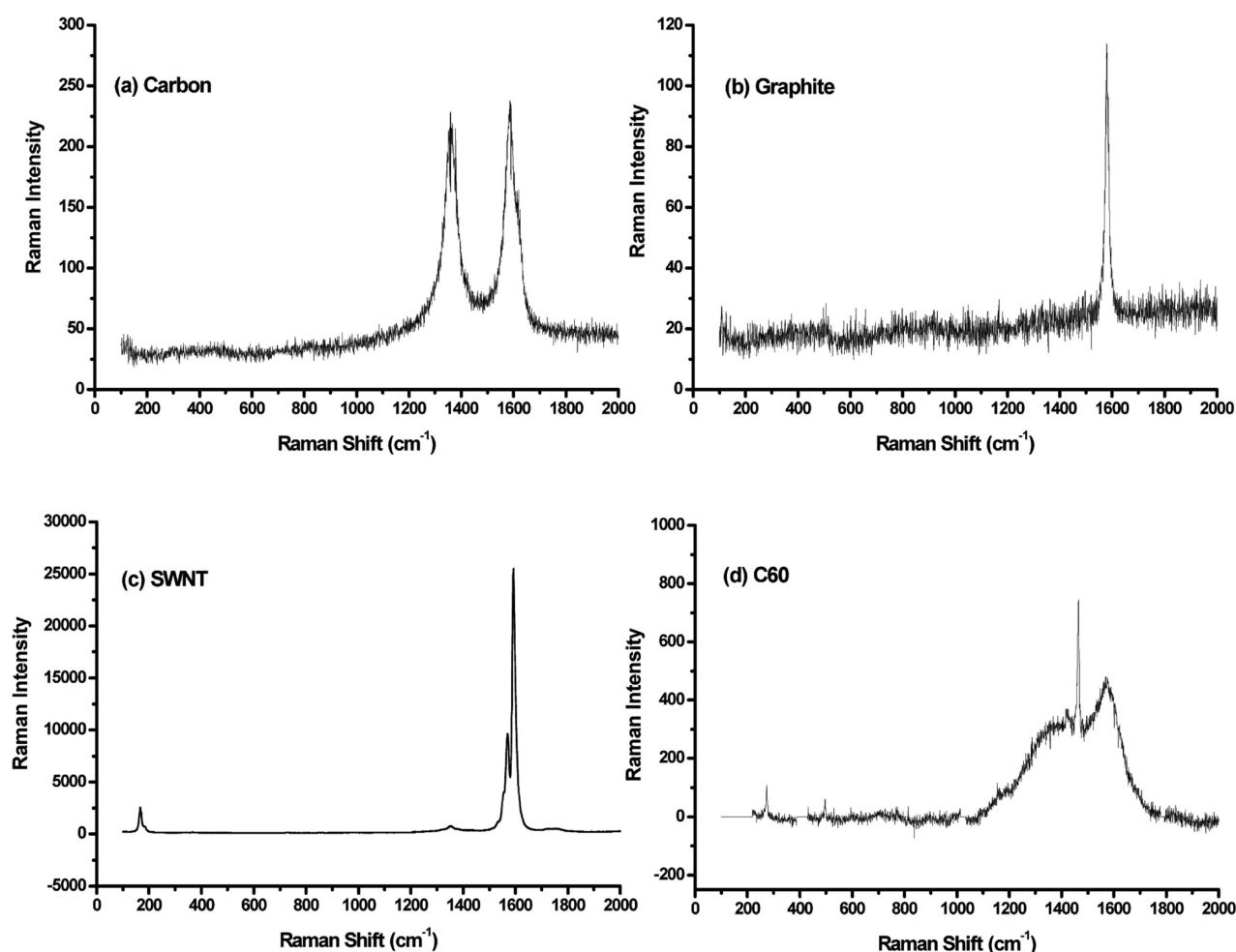
Figure 2. Raman spectra of various carbon materials obtained with 488 nm laser light at range of 100 to 2000 cm^{-1}.

3. RESULTS AND DISCUSSION

3.1. Morphology and Microstructure of Carbon Materials.

3.1.1. Morphology Characterization of Various Carbon Materials with Transmission Electron Microscopy (TEM). Figure 1 shows typical TEM images of the four selected carbon materials. In Figure 1(a), small round objects are attributed to the individual C_{60} molecules with the average size of 30 nm in out diameter, and large blocks are aggregated C_{60} groups. Figure 1(b) displays a TEM image of either single or bundled array of SWNTs. A rough value of the out diameter of 10−40 nm is estimated from single SWNTs. The images of edge planes of graphite and carbon samples were caught. Figure 1(c) clearly shows an obvious turbostratic orientation in a single carbon particle. A prefect parallel and equidistant layer orientation in graphite sample was observed in Figure 1(d), indicating ideal single crystal graphite without any irregularities within the graphene layers. The information obtained from TEM characterization is consistent with the result from Raman spectra as will be discussed later.

3.1.2. Microstructure Characterization on Various Carbon Materials with Raman Spectroscopy. Raman spectroscopy is sensitive to slight changes in microstructure of graphite materials; therefore, it is employed for the characterization of crystalline, nanocrystalline, and amorphous carbon phases. In addition, it is also sensitive enough to provide unique information about the

Table 3. Raman Spectrum Properties of Four Carbon Materials

sample no.	Raman G position (cm^{-1})	$I(D)/I(G)$	L_a (Å)	fwhm G (cm^{-1})
graphite	1579	0.086	613	12.2
carbon	1586	0.938	56	55.6
SWNT	1570	0.083	636	20.0
C_{60}	1568	0.640	83	120.0

similarities and differences among various carbon nanostructures. All carbon materials show common features in Raman spectra in the 800−2000 cm^{-1} region, in which the so-called G and D peaks at around 1560 and 1360 cm^{-1} are assigned to sp^2 orbital hybridization in π-conjugated rings structures. The G peak is due to the bond stretching of all pairs of sp^2 atoms in both ring and chains,[30] and the D band is symmetry forbidden in graphite, and its presence is associated with structure disorder.[31] The D- and G-bands are significant to give information about the electronic and geometric structure through the double resonance process, and the radial breathing mode (RBM) at low frequency region makes the diameter and the optical transition energy analysis of nanotubes possible.[13]

The Raman spectra of the four selected carbon materials are shown in Figure 2. There are two strong D-bands and G-bands

14573

dx.doi.org/10.1021/jp209013q |*J. Phys. Chem. A* 2011, 115, 14570–14580

appearing in the carbon sample, indicating that disordered structure dominates while a partial crystalline structure exists in the carbon sample as shown in Figure 2a. In contrast, the Raman spectrum of the graphite sample only shows a strong G-band, a typical Raman spectrum of single crystal graphite, which is consistent with a completely ordered (crystalline) structure of graphite as characterized with TEM (Figure 2b). Figure 2c
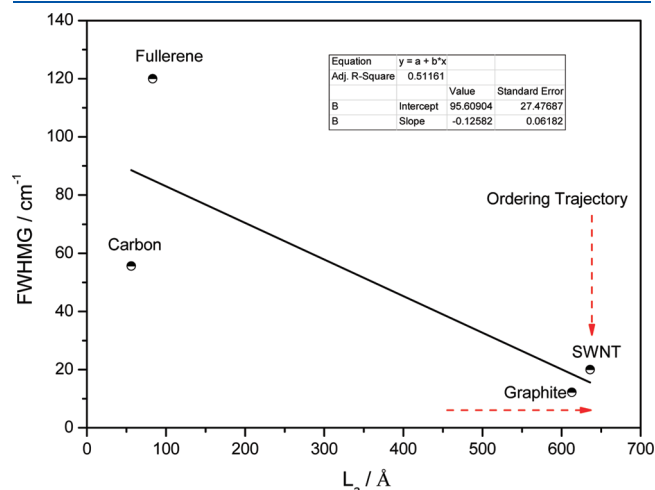
shows the typical Raman spectra of SWNTs, confirmed by three typical modes (i.e., the radial breathing modes (RBM) at ca. 180 cm^{-1}, the D-bond at 1350 cm^{-1} and the G-bond at ca. 1580 cm^{-1}). The peaks at the low-frequency region between 70 and 280 cm^{-1} correspond to the radial breathing modes (RBM) of nanotubes, with which the diameter distribution of SWNTs would be analyzed.[32] Therefore, the diameter D of 1.35 nm is calculated from the frequency ω of the peak at 166 cm^{-1} by using the equation $\omega = 223.75/D$ given by Bandow et al.[33] Experimental data on the RBM frequency taken by many researchers have been fit using the relation $\omega_{RBM} = A/D + B$, where $A = 227 \pm 0.3$ nmcm^{-1} and $B = 0.3 \pm 0.2$ cm^{-1},[34] with which the diameter value of 1.36 nm is obtained. Meanwhile, using an equation of $\omega = 234/D + 10$ that was proposed for single wall nanotube bundles after eliminating the frequency shift induced from the interaction among nanotubes,[35,36] an average diameter of 1.50 nm is calculated. Clearly, three diameter values obtained from various fitting equations are consistent each other and an overall average diameter of 1.41 nm must be reasonable and approximately close to the out diameter of observed by TEM images. As shown in Figure 2d, several peaks at 1200−1600 cm^{-1} appeared corresponding to the intense stretching vibrational modes and a peak at ca. 1468 cm^{-1} is characteristic signal for C$_{60}$ caused by A$_g$(2) mode. The unique properties in fullerene (C$_{60}$) are due to the highly delocalized and strongly correlated π-electrons in the spherical cage.[37]

Generally, G-bands and D-bands exist in all carbon samples and the crystallite size of carbon materials (L_a) could be
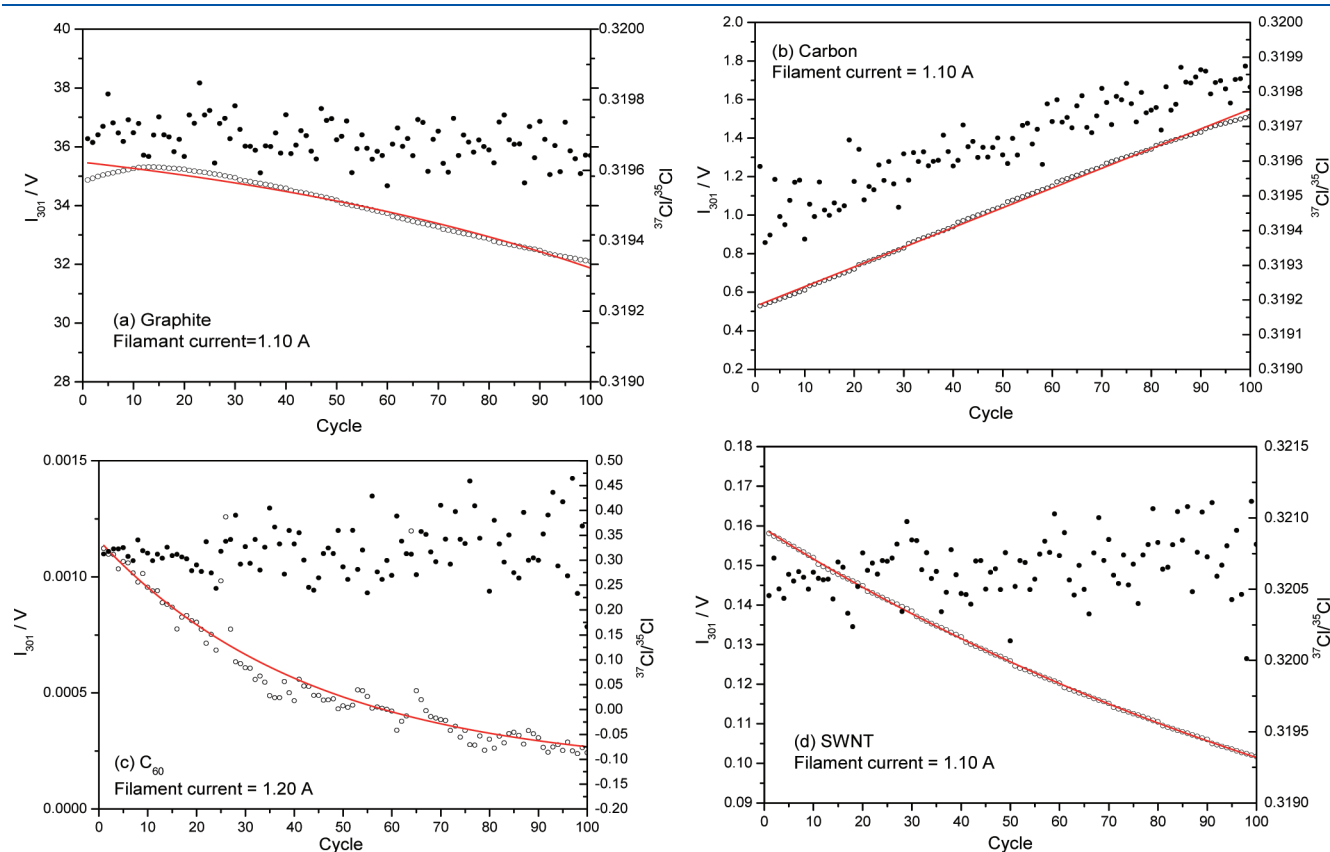

Figure 3. Plot of the full width at half-maximum of the G-peak (fwhm G) with decreasing in-plane crystallite size of L_a. Red dashed lines represent the ordering trajectory of the carbon materials.

Figure 4. Variation of the peak intensity and the ratios of ^{37}Cl/^{35}Cl obtained under 100 cycles of measurement by collecting the polyatomic ion Cs$_2$Cl$^+$ at a typical filament current in the presence of various carbon materials in PTIMS. Solid symbols are the determined ^{37}Cl/^{35}Cl ratios and open circles are the intensity of peak at m/e 301.

14574

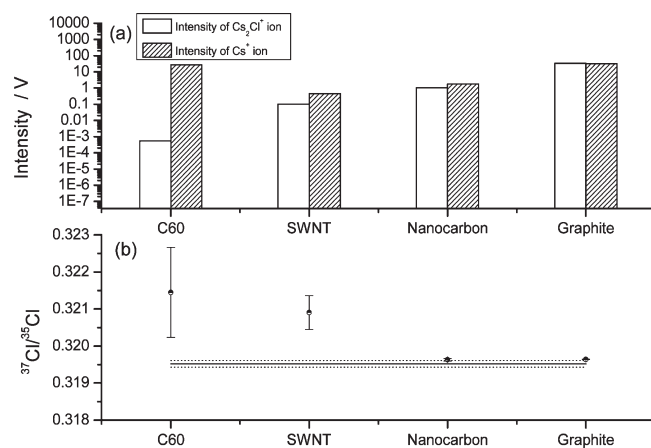dx.doi.org/10.1021/jp209013q |*J. Phys. Chem. A* 2011, 115, 14570–14580

Table 4. Intensity of Cs_2Cl^+ / $Cs_2BO_2^+$ Ion and Chlorine and Boron Isotopic Composition of Standard Reference Materials (NIST 975 and NIST 951) with Various Carbon Materials

carbon material	$Cs_2BO_2^+$ ion			Cs_2Cl^+ ion		
	filament current (mA)	intensity (V)	$^{11}B/^{10}B$	filament current (mA)	intensity (V)	$^{37}Cl/^{35}Cl$
fullerenes (C_{60})	1417	0.18	4.05616 ± 0.00043	1397	0.00055	0.320318 ± 0.000337
			4.05620 ± 0.00068			0.322736 ± 0.005470
			4.05196 ± 0.00022			0.321290 ± 0.012666
average			**4.05477 ± 0.00243**			**0.321448 ± 0.001217**
SWNTs	1250	0.53	4.05050 ± 0.00016	1163	0.10	0.321432 ± 0.000047
			4.05025 ± 0.00057			0.320637 ± 0.000242
			4.04988 ± 0.00011			0.320650 ± 0.000020
average			**4.05021 ± 0.00031**			**0.320906 ± 0.000455**
carbon	1300	0.32	4.04859 ± 0.00078	1100	1.04	0.319595 ± 0.000006
			4.04840 ± 0.00042			0.319642 ± 0.000008
			4.05319 ± 0.00091			0.319656 ± 0.000013
average			**4.05006 ± 0.00271**			**0.319631 ± 0.000032**
graphite	1381	1.4	4.05112 ± 0.00007	1103	34	0.319677 ± 0.000008
			4.05107 ± 0.00006			0.319685 ± 0.000005
			4.05106 ± 0.00008			0.319666 ± 0.000002
average			**4.05108 ± 0.00003**			**0.319676 ± 0.000009**
previous results			**4.0506 ± 0.0007**[a]			**0.319519 ± 0.000089**[b]

[a] $^{11}B/^{10}B$ value of 4.0506 ± 0.0007 determined by S. Tonarini et al. using $Cs_2BO_2^+$-graphite-PTIMS method.[40] [b] $^{37}Cl/^{35}Cl$ value of 0.319519 ± 0.000089 given by Y.K Xiao et al. using Cs_2Cl^+-graphite-PTIMS.[41]
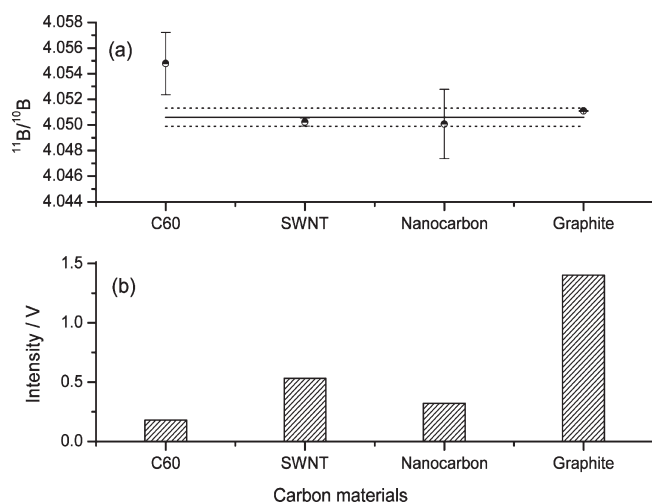
Figure 5. Determined boron isotopic ratios of $^{11}B/^{10}B$ (a) and intensity of peak $^{133}Cs_2{}^{11}B^{16}O_2^+$ ions (b) obtained from NIST 951 solution containing 1 μg of boron in the presence of various carbon materials. Solid line represents the previously reported data for $^{11}B/^{10}B$ ratio in NIST 951.[40]

Figure 6. (a) Intensity of peak $^{133}Cs_2{}^{35}Cl^+$ ions and (b) determined chlorine isotopic ratios of $^{37}Cl/^{35}Cl$ obtained from NIST 975 containing 1 μg of chlorine in the presence of various carbon materials. Solid line represents the previously reported data for $^{37}Cl/^{35}Cl$ ratio in NIST 975.[41]

estimated from the TK rule, i.e., $I(D)/I(G) \propto 1/L_a$.[38] The full width at half-maximum of G peak (fwhm G) is a critical index for the extent of disordering of carbon materials as it increases with increasing disorder, as reported by Ferrari et al.[39] The Raman spectrum properties of four carbon materials are listed in Table 3. The plot of fwhm G vs L_a gives the plane ordering sequence of all carbon materials: Graphite > SWNT > Carbon > Fullerene, confirming that Raman spectrum properties really reflect the actual structure of the selected carbon materials. Both SWNT and

graphite with sp^2 hybridized C—C bond graphene sheets have similar in-plane crystallite size values (i.e., L_a), but the fwhm G value of SWNT is larger than that of graphite, reflecting the curling graphene sheets in SWNT. At another end-member of the trend line in Figure 3, the extent of disordering in carbon is better than that of C_{60} because of partial graphene sheets existing in carbon.

3.2. Emission of Polyatomic Ions in the Presence of Various Carbon Materials. *3.2.1. Emission of $Cs_2BO_2^+$ and Cs_2Cl^+ Ions in Positive Thermal Ionization Mass Spectrometry.* To further explore the formation mechanism of those polyatomic ions in the ioniza-
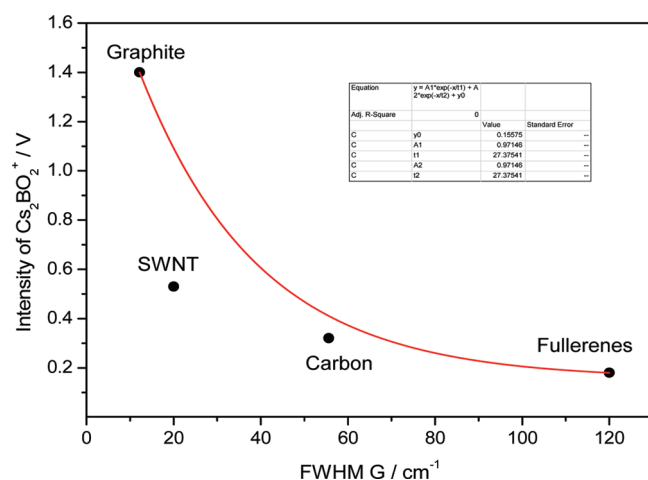
Figure 7. Dependence of emission capacity of $Cs_2BO_2^+$ ions on the extent of disordering in plane structure in carbon materials (i.e., fwhm G).

Figure 8. Dependence of emission capacity of Cs_2Cl^+ ions on the extent of disordering in plane structure in carbon materials (i.e., fwhm G). Y axis is in the common logarithm scale.

tion source of thermal ionization mass spectrometry (TIMS), the emission behavior of two polyatomic ions (i.e., $Cs_2BO_2^+$ and Cs_2Cl^+) with the four typical carbon materials are compared in this study. Here, the stable emission behavior of polyatomic Cs_2Cl^+ ion with four selected carbon materials under 100 cycles of measurement (around 15 min) are shown in Figure 4. The average peak intensity at m/e 301 (i.e., $^{133}Cs_2{}^{35}Cl^+$) with graphite is one- and/or two-orders of magnitude higher than that with nanocarbon and SWNT even though the signal of Cs_2Cl^+ ion decays slowly slightly with graphite. The peak signal with fullerenes (C_{60}) is dramatically low and cannot keep stable emission even at higher ionization temperature. With the exception of carbon promoter samples with which the peak intensity of peak at m/e 301 increases with time as fitted by an linear equation in Figure 4b, the intensity of peak ion signals of m/e 301 with graphite, SWNTs, and C_{60} shows a declining trend, and the curves of peak intensity of m/e 301 with time (i.e., I_{301} vs cycle) are well described by the exponential decay function (Figure 4a,c,d). In addition, the variation of $^{37}Cl/^{35}Cl$ ratios from 100 cycles with various carbon materials is also compared in Figure 4. The ratios of $^{37}Cl/^{35}Cl$ obtained with graphite almost keep a constant during 100 cycles of data collection, and the highest internal-precision of 0.03‰ is obtained. The ratios of $^{37}Cl/^{35}Cl$ obtained with SWNTs and nanocarbon increase with time, and that with C_{60} ranged from 0.24 to 0.46 is completely unreliable. Meanwhile, the variation of the peak intensity and the ratios of $^{11}B/^{10}B$ obtained under 100 cycles of measurement by collecting the polyatomic ion $Cs_2BO_2^+$ also were checked (not shown in the text). It also presents the obvious difference in the peak intensity and the $^{11}B/^{10}B$ ratios with different carbon materials, indicating the microstructure effect on the emission behavior of $Cs_2BO_2^+$ ion.

Therefore, we concluded that the graphite with perfect parallel and equidistant layer orientation benefits the formation and the stable emission of those polyatomic ions in the source of TIMS, and SWNT with curl plane structure and carbon with partial parallel layers is inferior to graphite but greatly superior to C_{60} that has the mixed phase of face-centered cubic (fcc) and hexagonal close-packed structure.

As is well-known, the stable emission of single/polyatomic ions with high intensity is essential to ensure high-precision determination of isotopic composition by TIMS, the accuracy and precision of determined boron and chlorine isotopic compositions in
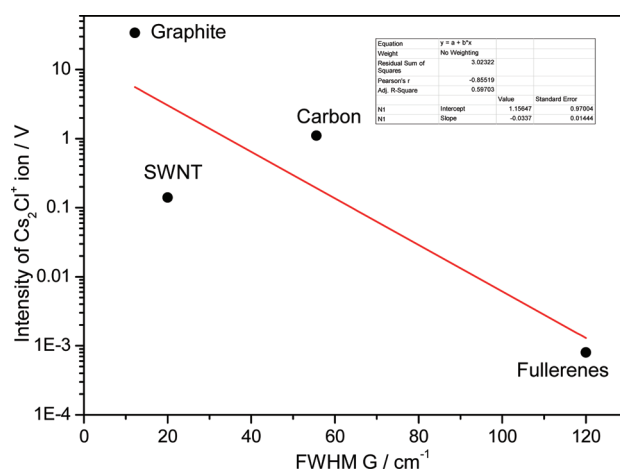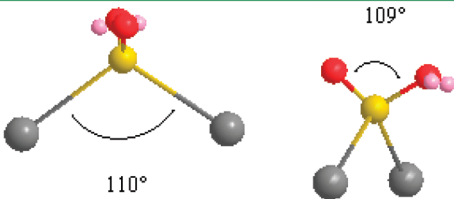
two standard reference materials (NIST 951 and NIST 975) was evaluated in this work. Boron isotopic composition of $^{11}B/^{10}B$ obtained from the ratio of 309/308 (i.e., $^{11}B/^{10}B = R_{309/308} - 0.00079$) and chlorine isotopic composition of $^{37}Cl/^{35}Cl$ from the ratio of 303/301 (i.e., $^{37}Cl/^{35}Cl = R_{303/301}$) by detecting $Cs_2BO_2^+$ ion and Cs_2Cl^+ ion are compared in Table 4 and Figures 5 and 6.

Our previous investigation proved that no peak of Cs_2Cl^+ can be observed except for the very strong emission of Cs ion in the absence of any carbon materials.[26] Meanwhile, the intensity of $Cs_2BO_2^+$ ions with graphite is two-orders of magnitude higher than the emission without any carbon materials, which has been investigated in detail by Xiao et al.[8]

Obviously, the intensity of $Cs_2BO_2^+$ ion is affected by carbon promoters as shown in Figure 5(b). The determined $^{11}B/^{10}B$ values by employing $Cs_2BO_2^+$ ion using carbon, SWNTs, and graphite are roughly consistent with the previous result given by Tonarini et al., and that of C_{60} with a larger relative standard deviation (RSD) deviates far from others. An overall uncertainty of 0.01‰ (1s) on boron isotopic ratio for NIST 951 containing 1 μg of boron can be achieved in the presence of graphite. On the basis of the difference in the peak intensity and precision of $^{11}B/^{10}B$ determined, it is clear that the emission capacity of four selected carbon materials for $Cs_2BO_2^+$ ion is distinguishing and the general sequence is as follows: Graphite > SWNT > carbon > C_{60}. The same phenomenon for the emission capacity of Cs_2Cl^+ ion also was observed with various carbon materials as shown in Figure 6, and the intensity of Cs_2Cl^+ with C_{60} is dramatically lower than that with other carbon materials. Correspondingly, the determined $^{37}Cl/^{35}Cl$ ratio by C_{60} is far away from the given value and the emission capacity follows the order: Graphite > carbon > SWNT > C_{60}. To address the formation mechanism of polyatomic ions in TIMS, the intensity of single Cs^+ ion is compared with that of polyatomic Cs_2Cl^+ ion in the presence of typical carbon materials. In Figure 6(a), the intensity ratio of Cs_2Cl^+ to Cs^+ with graphite is close to 1.1 (i.e., 34 V/32 V), and that with C_{60} is around 2.0×10^{-5}, which indicates that equal proportion of single ions and polyatomic ions are produced with graphite sample and only a few polyatomic ions are emitted with C_{60}. The general sequence for intensity ratio of Cs_2Cl^+ to Cs^+ is as follows: Graphite > nanocarbon > SWNT > C_{60}.

Table 5. Optimized Structure, Bond Length, Bond Angles, And Minimum Energy of Cs_2Cl^+ and $Cs_2BO_2^+$ Ions in Gas Phase
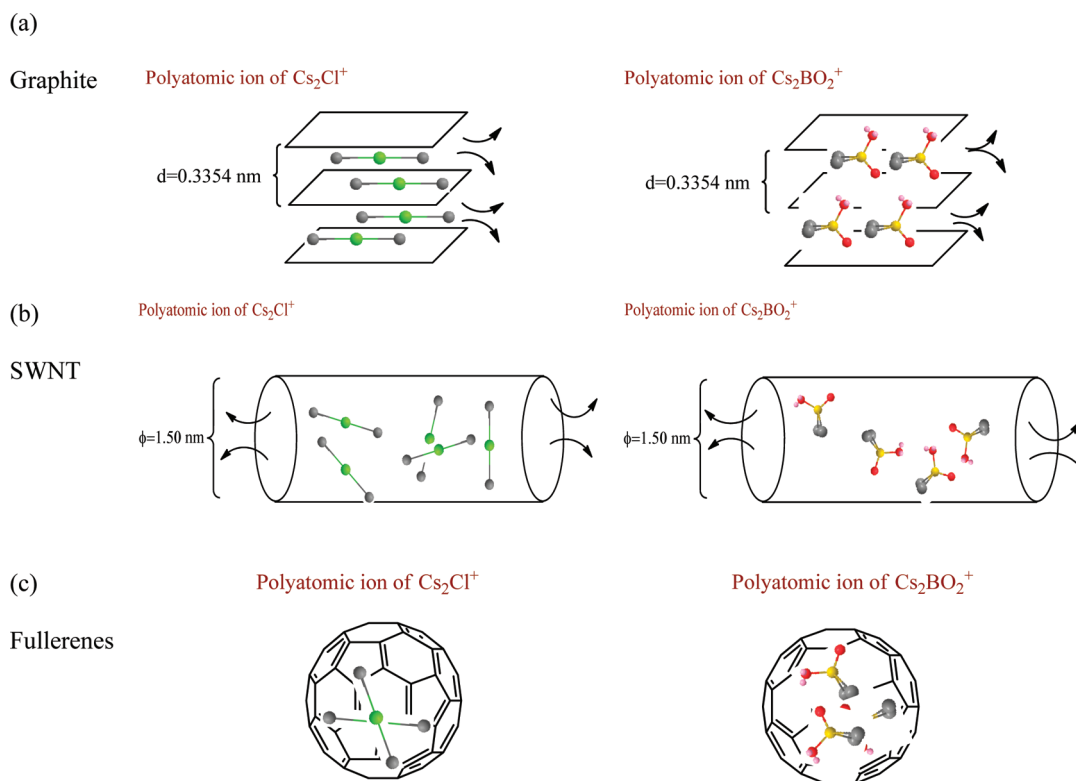
Cs_2Cl^+ ion	$Cs_2BO_2^+$ ion

Bond Length:

    Cs(1)-Cl(2): 3.3157 Å

    Cl(2)-Cs(3): 3.3157 Å

Bond Angle: 180^0

Total Energy: 494.9578 kcal/mol

Bond Length:

B-Cs: 3.1744 Å   B-O: 1.4645 Å

B-O(with lone pair): 1.6573 Å

Bond Angle:

Cs-B-Cs: 109.5997^0

Cs-B-O (Average): 109.4338^0

O-B-O: 109.4920^0

Lp-O-Lp: 109.4431^0 (Lp represents lone pair)

Total Energy: 8.2937 kcal/mol

Scheme 1. (a) Diagram of Surface Ionization Reaction of CsCl and $Cs_2B_4O_7$ on Heating Filament in the Absence of Any Carbon Promoter; (b) Proposed Mechanism of the Formation of Polyatomic Ions (Cs_2Cl^+ and $Cs_2BO_2^+$) in the Presence of Graphite
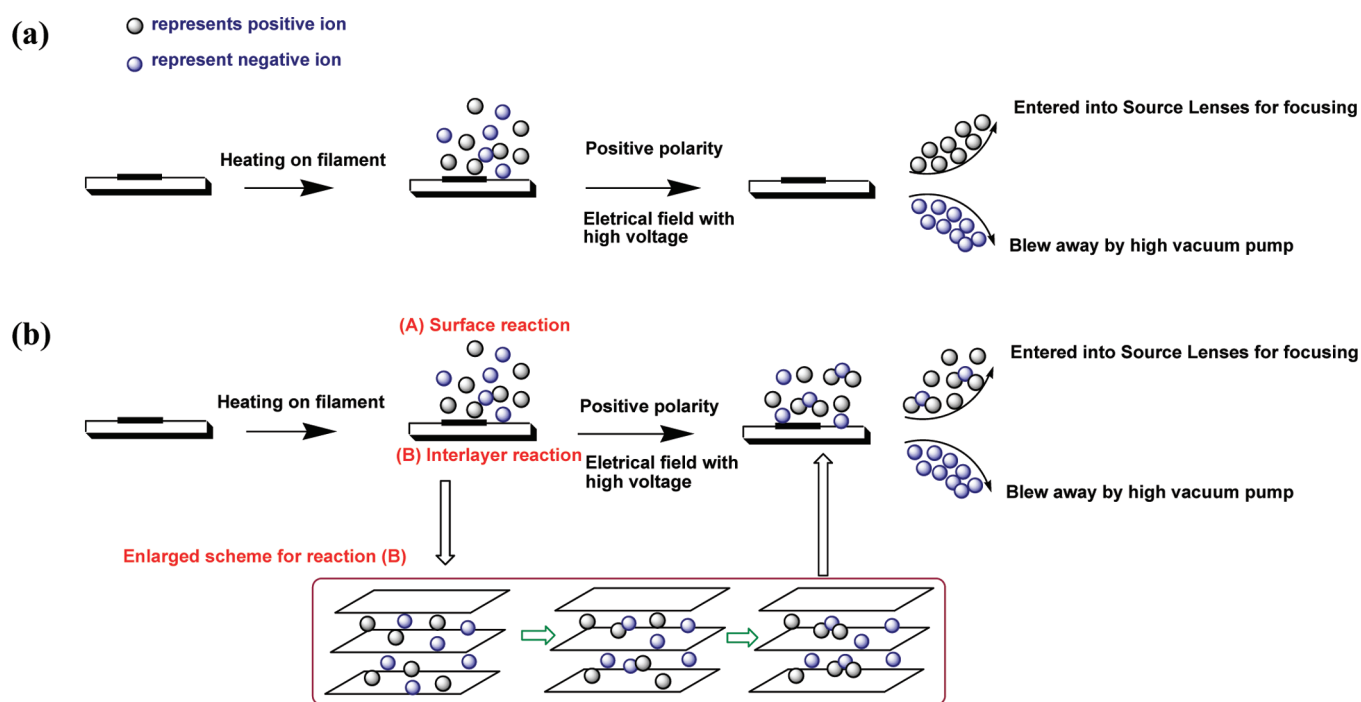
3.2.2. Relationship between the Emission Capacity of Polyatomic Ions and the Microstructure of Various Carbon Materials. The results from the above section confirmed the dependence of the emission behavior of polyatomic ions on the microstructure of various carbon materials. As shown in Figures 7 and 8, the plots of fwhm vs intensity of $Cs_2BO_2^+/Cs_2Cl^+$ ions give a quantitative expression for the trend: the higher the extent of disordering in plane structure of carbon materials, the worse emission capacity for polyatomic ions in TIMS becomes. The intensity of Cs_2Cl^+ with carbon is obviously stronger than with SWNT, whereas that of

$Cs_2BO_2^+$ with SWNT is around two-times greater than with carbon reversely, which would be explained by two reasons: (1) compared with $Cs_2BO_2^+$ ion, the emission of Cs_2Cl^+ ion is very sensitive to the carbon materials used, and the rolled single graphite sheets would hinder the emission of Cs_2Cl^+ with linear structure; (2) partial ideal graphene sheets exist in carbon powder as observed in TEM images, and the local heterogeneity in carbon microstructure would cause the accidental phenomenon. Therefore, graphite and C_{60} lie on the two end-members, respectively, and SWNT and carbon stand at the middle position in the emission capacity trend.

Scheme 2. Schematic Diagram of Structure Effects of Three Typical Carbon Materials on the Emission of Polyatomic Ions in the Ionization Source of TIMS

(a)

Graphite   Polyatomic ion of Cs_2Cl^+ Polyatomic ion of $Cs_2BO_2^+$

d=0.3354 nm   d=0.3354 nm

(b)

SWNT   Polyatomic ion of Cs_2Cl^+ Polyatomic ion of $Cs_2BO_2^+$

ϕ=1.50 nm ϕ=1.50 nm

(c)

Fullerenes   Polyatomic ion of Cs_2Cl^+ Polyatomic ion of $Cs_2BO_2^+$

3.3. Proposed Mechanism for the Formation of Polyatomic Ions in the Presence of Various Carbon Materials in TIMS. *3.3.1. Configuration of Cs_2Cl^+ and $Cs_2BO_2^+$ Polyatomic Ions in Gas Phase.* Prior to the discussion on the formation mechanism of polyatomic ions in ionization source of TIMS, the configurations of Cs_2Cl^+ and $Cs_2BO_2^+$ in gas phase are explored. The initial structures of Cs_2Cl^+ and $Cs_2BO_2^+$ are prepared using ChemDraw and Chem3D software (CambridgeSoft, version 12.0), and the geometry optimization is carried out using the default molecular dynamics MM2 force field parameters in Chem3D. The optimized structures including structure parameters, bond length, bond angles, and the minimum energy for Cs_2Cl^+ and $Cs_2BO_2^+$ ions in gas phase are listed in Table 5. The optimal configurations of Cs_2Cl^+ and $Cs_2BO_2^+$ ions are highly symmetrical, and a linear structure with a total length of 6.6 Å for Cs_2Cl^+ ion and a tetrahedral structure for $Cs_2BO_2^+$ ion are obtained, which means the polyatomic ion of $Cs_2BO_2^+$ is more flexible at electric/magnetic field because of its small steric hindrance effect. The minimum energy of 8.3 kcal/mol for $Cs_2BO_2^+$ ion is almost two-orders of magnitude lower than that of Cs_2Cl^+ ion (i.e., 495 kcal/mol) in gas phase as given by the molecular dynamic calculation, indicating the polyatomic ion $Cs_2BO_2^+$ is more stable than Cs_2Cl^+ ion in the ionization source. It might explain the experimental phenomenon that $Cs_2BO_2^+$ ion easily formed in the ionization source of TIMS even though at the condition without any carbon promoter, while the polyatomic ion Cs_2Cl^+ could not be observed except for a very strong signal of Cs^+ ion in the absence of any carbon promoter and the stability of Cs_2Cl^+ ion is very sensitive to the micro structure property of carbon materials.

3.3.2. Proposed Mechanism for Formation of Polyatomic Ions (Cs_2Cl^+ and $Cs_2BO_2^+$) in the Ionization Source of TIMS. Both positively charged and negative charged ions will be formed by surface ionization on a heating filament in the ionization source of TIMS. Unlike the formation of ion clusters in ESI or ICP-MS, the dissociation reaction of CsX (X represents Cl and BO_2) only produces Cs^+ and X^- on a heated filament in TIMS. When high voltage electrical field with positive polarity is applied, only positively charged ions could be detected while negatively charged ions is blown away by high vacuum pump as shown in Scheme 1(a). Oppositely, there are only negatively charged ions detected if the accelerating voltage is switched to negative mode (not shown here). On the basis of the comparable studies in Section 3.2 showing the function of graphene sheets on the formation of polyatomic ions in TIMS, the proposed mechanism for the formation of polyatomic ions is given in Scheme 1(b). First, partial positively/negatively charged ions emit from the surface of filament directly after surface ionization reaction, while others stay at interlayer of graphene sheets caused by interaction between charged ions and graphite sheets. Second, a surface-induced collision occurs between charged ions at the interlayer of graphene sheets where one positive ion (i.e., Cs^+) attracts one negative ion (i.e., Cl^- or BO_2^-) by electrostatic attraction because the transitory stay of charged ions in carbon materials provides the opportunity to charged ions to meet each other. Third, the ion-pair would attract the third positive ion because of dipole polarization in ionic bonds. Therefore, both single positive charged ions (i.e., Cs^+) and polyatomic positive charged ions (Cs_2Cl^+ and $Cs_2BO_2^+$ ions) could be detected by TIMS. In general, atomic ions (i.e., Cs^+, Cl^-, or BO_2^-) escape from the surface of ionization filament immediately in the absence of any carbon promoter, while the existence of graphene sheets provides space for collision reaction among single charged ions and the surface-induced collision benefit the formation of polyatomic ions as a result. However, the yield of

polyatomic ions is very sensitive to microstructure of carbon promoter employed as stressed on Section 3.2, and possible explanation will be given in Section 3.3.3.

3.3.3. Structure Effects of Carbon Materials on the Emission of Polyatomic Ions. Both the minor difference in graphite samples and the major discrepancy in microstructure among various carbon materials strongly affects the formation and the emission of polyatomic ions in the ionization source of TIMS, which raises questions as to how the microstructure of carbon materials relate to their emission capacity for polyatomic ions. As discussed above, the stable configuration of Cs_2Cl^+ and $Cs_2BO_2^+$ are linear and tetrahedral in the gas phase, respectively (Table 5), and the combination of the geometry of the selected four carbon materials with the configuration of two polyatomic ions might explain the experimental observations. (1) Graphite with the interlayer distance of ~3.354 Å only allow Cs_2Cl^+ and $Cs_2BO_2^+$ ions emit from the graphene layer with certain orientations as shown in Scheme 2(a). As the number of orientation of charged polyatomic ions in interlayer of graphite are limited, the distortion in graphene layers affects the stability/intensity of polyatomic ions. Thus, graphite samples with perfectly parallel and equidistant layers ensure the emission capacity for polyatomic ions to the maximum extent. Obviously, the linear configuration of Cs_2Cl^+ is less flexible than that of $Cs_2BO_2^+$ ion in gas phase, therefore the emission of the ions is very sensitive to the microstructure of carbon materials used. (2) Carbon with turbostratic stacked sheets worsens the emission as a result of blocking the emission pathway of polyatomic ions. However, the existence of partial parallel oriented sheets in carbon would give better performance, such as the result shown in Figure 6, but it is not true for all carbon samples and only happens occasionally. (3) SWNTs with rolled single graphene sheet might act in the same function for the formation of polyatomic ions as graphite, but the pathway of ion emission is restricted by its unique structure of SWNTs (Scheme 2(b)). The SWNT sample with the average diameter of 14.1 Å provides enough space for emission of two polyatomic ions from two-end of one single-walled nanotube with any possible orientation, and both Cs_2Cl^+ and $Cs_2BO_2^+$ ions cannot permeate through the wall because the size of two ions is larger than single hexagon ring. (4) Fullerenes with closed ball structure might seal the polyatomic ions produced inside of the ball (Scheme 2(c)), which has been proved by the pretty weak signal of polyatomic ions compared with the signal obtained from graphite.

4. CONCLUSIONS

The emission behavior of polyatomic ions (i.e., Cs_2Cl^+ and $Cs_2BO_2^+$ ions) with four typical carbon materials (Graphite, Carbon, SWNTs, and Fullerenes) in the ionization source of TIMS has been investigated, and the results indicate that the emission behavior of two polyatomic ions strongly depends on microstructure of carbon materials used. A good correlation between the extent of disordering in plane structure and the emission capacity of polyatomic ions provides a helpful clue to understand the mechanism for the formation of such polyatomic ions. Consequently, a possible mechanism for the formation of polyatomic ions has been proposed based on the configuration of two ions in gas phase, and the structure effects of carbon material on the emission of those ions have been discussed as well.

After roughly investigating the morphology of four selected carbon materials by TEM, the unique information about the similarities and differences among various carbon nanostructures

has been characterized using Raman spectroscopy. An average diameter of 1.41 nm for SWNT calculated from the radial breathing mode (RBM) at low frequency region of Raman spectra approximately close to the out diameter of observed by TEM images, and the typical Raman spectra properties reflects actual structure of the selected carbon materials, and the plane ordering sequence of all carbon materials is the following: Graphite > SWNTs > Carbon > Fullerene.

The emission behavior of two polyatomic ions ($Cs_2BO_2^+$ and Cs_2Cl^+) in the presence of four selected carbon materials has been studied by comparing the signal intensity of $Cs_2BO_2^+$ and Cs_2Cl^+ ions and the precision/accuracy of determined isotopic composition of chlorine and boron in two international standard reference materials (NIST 975 and NIST 951) using PTIMS-$Cs_2BO_2^+$ and PTIMS-Cs_2Cl^+ methods. The results show that the emission capacities of the selected carbon materials for $Cs_2BO_2^+$ ion and Cs_2Cl^+ ion are Graphite > SWNTs > carbon > C_{60} and Graphite > carbon > SWNT > C_{60}, respectively. The general capacity trend that graphite followed by SWNTs or carbon is dramatically superior to C_{60} is consistent with the disordering extent in plane structure of carbon materials as characterized by Raman spectroscopy.

On the basis of the optimized configuration of $Cs_2BO_2^+$ and Cs_2Cl^+ ions in gas phase using a molecular dynamics method, a surface-induced collision mechanism for formation of polyatomic ions in the ionization source of TIMS has been proposed by three steps: (1) Escape of single ions is slowed down by retarding effect occurred between single charged ions and graphene layers; (2) Two opposite charged ions attracts each other by electrostatic attraction among graphene layers; and (3) Attachment of the third positively charged single ion to the ion-pair occurs as induced by dipole moment. The combination of the geometry of the selected carbon materials with the configuration of two polyatomic ions explains the structure effect of carbon materials on the emission behavior of polyatomic ions. Graphite samples with perfectly parallel and equidistant layers ensure the capacity of emission to the maximum extent because the orientation of charged polyatomic ions in interlayer of graphite are limited, and the distortion in graphene layers affects the stability/intensity of polyatomic ions. Carbon with turbostratic stacked sheets worsens the emission as a result of blocking the emission pathway of polyatomic ions. SWNTs provide enough space for emission of two polyatomic ions from two-ends of one single-walled nanotube with any possible orientation, but the capacity of ion emission is restricted by its unique structure in which both Cs_2Cl^+ and $Cs_2BO_2^+$ ions cannot permeate through the wall. Fullerenes give the worst performance because the closed ball structure seals all polyatomic ions inside of the ball.

■ AUTHOR INFORMATION

Corresponding Author
*Phone: +86 (25) 83596832; Fax: +86 (25) 83592393; E-mail: shyjiang@nju.edu.cn.

■ REFERENCES

(1) Sears, K. C.; Ferguson, J. W.; Dudley, T. J.; Houk, R. S.; Gordon, M. S. *J. Phys. Chem. A* **2008**, *112*, 2610.

(2) Jasık, J.; Zyabka, J.; Feketeova, L.; Ipolyi, I.; Mark, T. D.; Herman, Z. *J. Phys. Chem. A* **2005**, *109*, 10208.

(3) Laramhe, J. A.; Hemberger, P. H.; Cooks, R. *J. Am. Chem. Soc.* **1979**, *101* (21), 6460.

(4) Qayyum, A.; Herman, Z.; Tepnual, T.; Mair, C.; Matt-Leubner, S.; Scheier, P.; Mark, T. D. *J. Phys. Chem. A* **2004**, *108* (1), 1.

(5) Thode, H. G.; MacNamara, J.; Lossing, F. P.; Collins, C. B. *J. Am. Chem. Soc.* **1948**, *70*, 3008.

(6) Ramakumar, K. L.; Parab, A. R.; Khodade, P. S.; Almaula, A. I.; Chl-tambar, S. A; Jain, H. C. *J. Radianal. Nucl. Chem.* **1985**, *94*, 53.

(7) Spivack, A. J.; Edmond, J. M. *Anal. Chem.* **1986**, *58*, 31.

(8) Xiao, Y. K.; Beary, E. S.; Fassett, J. D. *Int. J. Mass Spectrom. Ion Proc.* **1988**, *85*, 203.

(9) Aggarwalt, J. K.; Palmer, M. R. *Analyst* **1995**, *120*, 1301.

(10) Xiao, Y. K.; Zhang, C. G. *Int. J. Mass Spectrom. Ion Proc.* **1992**, *116*, 183.

(11) Xiao, Y. K.; Liu, W. G.; Qi, H. P.; Zhang, C. G. *Int J. Mass Spectrom. Ion Proc.* **1993**, *123*, 117.

(12) Xiao, Y. K.; Yin, D. Z.; Lu, H. *Chin. J. Salt Lake Res.* **2001**, *9* (3), 17.

(13) Dresselhaus, M. S.; Jorio, A.; Hofmann, M.; Dresselhaus, G.; Saito, R. *Nano Lett.* **2010**, *10*, 751.

(14) Radovic, L. R. *Chemistry and Physics of Carbon*; Dekker: New York, 1994, Vol 24.

(15) Zheng, Q.; Xue, Q.; Yan, K.; Hao, L.; Li, Q.; Gao, X. *J. Phys. Chem. C* **2007**, *111*, 4628.

(16) Radovic, L. R.; Bockrath, B. *J. Am. Chem. Soc.* **2005**, *127*, 5917.

(17) Nakanishi, T.; Miyashita, N.; Michinobu, T.; Wakayama, Y.; Tsuruoka, T.; Ariga, K.; Kurth, D. G. *J. Am. Chem. Soc.* **2006**, *128*, 6328.

(18) Kayiran, S. B.; Lamari, F. D.; Levesque, D. *J. Phys. Chem. B* **2004**, *108*, 15211.

(19) Kam, N. W. S.; Jessop, T. C.; Wender, P. A.; Dai, H. J. *J. Am. Chem. Soc.* **2004**, *126*, 6850.

(20) Kam, N. W. S.; Dai, H. J. *J. Am. Chem. Soc.* **2005**, *127*, 6021.

(21) Pantarotto, D.; Briand, J.; Prato, M.; Bianco, A. *Chem. Commun.* **2004**, *1*, 16.

(22) Lu, Q.; Moore, J. M.; Huang, G.; Mount, A. S.; Rao, A. M.; Larcom, L. L.; Ke, P. C. *Nano Lett.* **2004**, *4*, 2473.

(23) Cherukuri, P.; Bachilo, S. M.; Litovsky, S. H.; Weisman, R. B. *J. Am. Chem. Soc.* **2004**, *126*, 15638.

(24) Bianco, A.; Hoebeke, J.; Godefroy, S.; Chaloin, O.; Pantarotto, D.; Briand, J. P.; Muller, S.; Prato, M.; Partido s, C. D. *J. Am. Chem. Soc.* **2005**, *127*, 58.

(25) Tezuka, N.; Umeyama, T.; Seki, S.; Matano, Y.; Nishi, M.; Hirao, K.; Imahori, H. *J. Phys. Chem. C* **2010**, *114*, 3235.

(26) Wei, H. Z.; Jiang, S. Y.; Xiao, Y. K. *J. Phys. Chem. A* **2010**, *114*, 2427.

(27) Nakamura, E.; Ishikawa, T.; Birck, J. L. *Chem. Geol.* **1992**, *94*, 193.

(28) Nakano, T.; Nakamura, E. *Int. J. Mass Spectrom.* **1998**, *176*, 13.

(29) Jiang, S. Y.; Wei, H. Z. 201010509775.3, 2010.

(30) Ferrari, A. C.; Rodil, S. E.; Robertson. *J. Phys. Rev. B* **2003**, *67*, 155306.

(31) Muradov, N.; Smith, F.; Bokerman, G. *J. Phys. Chem. C* **2009**, *113*, 9737.

(32) Kayiran, S. B.; Lamari, F. D.; Levesque, D. *J. Phys. Chem. B* **2004**, *108*, 15211.

(33) Bandow, S.; Asaka, S.; Saito, Y.; Rao, A. M.; Grigorian, L.; Richter, E.; Eklund, P. C. *Phys. Rev. Lett.* **1998**, *80*, 3779.

(34) Jorio, A.; Saito, R.; Hafner, J. H.; Lieber, C. M.; Hunter, M.; McClure, T.; Dresselhaus, G.; Dresselhaus, M. S. *Phys. Rev. Lett.* **2001**, *86*, 1118.

(35) Kuzmany, H.; Plank, W.; Hulman, M.; Kramberger, Ch.; Cruneis, A.; Pichler, T.; Peterlik, H.; Kataura, H.; Achiba, Y. *Eur. Phys. J. B* **2001**, *22*, 307.

(36) Milnera, M.; Kurti, J.; Hulman, M.; Kuzmany, H. *Phys. Rev. Lett.* **2000**, *84*, 1324.

(37) Katsuyoshi, I.; Kohei, U. *J. Phys. Chem. A Lett.* **2008**, *112*, 790.

(38) Tuinstra, F.; Koening, J. L. *J. Chem. Phys.* **1970**, *53*, 1126.

(39) Ferrari, A. C.; Robertson *J. Phys. Rev. B* **2001**, *64*, 075414.

(40) Tonarini, S.; Pennisi, M.; Leeman, W. P. *Chem. Geol.* **1997**, *142*, 129.

(41) Xiao, Y. K.; Zhou, Y. M.; Wang, Q. Z.; Wei, H. Z.; Liu, W. G.; Eastoe, C. J. *Chem. Geol.* **2002**, *182*, 655.

14580

dx.doi.org/10.1021/jp209013q |*J. Phys. Chem. A* 2011, 115, 14570–14580